Virus Research 228 (2017) 90–101

Contents lists available at ScienceDirect

Virus Research

journal homepage: www.elsevier.com/locate/virusres

Comparison analysis of microRNAs in response to EV71 and CA16 infection in human bronchial epithelial cells by high-throughput sequencing to reveal differential infective mechanisms

Yajie Hu, Jie Song, Longding Liu, Jing Li, Beibei Tang, Ying Zhang, Jingjing Wang, Lichun Wang, Shengtao Fan, Ming Feng, Qihan Li*

Institute of Medical Biology, Chinese Academy of Medical Science and Peking Union Medical College, Kunming, 650118, China

ARTICLE INFO

Article history:
Received 11 October 2016
Received in revised form
22 November 2016
Accepted 22 November 2016
Available online 24 November 2016

Keywords:
Enterovirus 71 (EV71)
Coxsackievirus A16 (CA16)
High-throughput sequencing
MicroRNAs (miRNAs)
Human bronchial epithelial (16HBE) cells

ABSTRACT

Hand, foot, and mouth disease (HFMD) mainly caused by Enterovirus 71 (EV71) and coxsackievirus A16 (CA16) infections which presented significantly different clinical manifestations. Nevertheless, the factors underlying these differences remain unclear. Recently, the functions of microRNAs (miRNAs) in pathogen-host interactions have been highlighted. Here, we performed comprehensive miRNA profiling in EV71- and CA16-infected human bronchial epithelial (16HBE) cells at multiple time points using high-throughput sequencing. The results showed that 154 known and 47 novel miRNAs exhibited remarkable differences in expression. Of these, 65 miRNAs, including 58 known and 7 novel miRNAs, presented opposite trends in EV71- and CA16-infected samples. Subsequently, we mainly focused on the 56 known differentially expressed miRNAs by further screening for targets prediction. GO and pathway analysis of these targets demonstrated that 18 biological processes, 7 molecular functions, 1 cellular component and 123 pathways were enriched. Among these pathways, Cadherin signalling pathway, Wnt signalling pathway and angiogenesis showed significant alterations. The regulatory networks of these miRNAs with predicted targets, GOs, pathways and transcription factors were determined, which suggested that miRNAs displayed intricate regulatory mechanisms during the infection phase. Consequently, we specifically analysed the hierarchical GO categories of the predicted targets involved in adhesion. The results indicated that the distinct changes induced by EV71 and CA16 infection may be partly linked to airway epithelial barrier function. Taken together, our data provide useful insights that help elucidate the different host-pathogen interactions following EV71 and CA16 infection and might offer novel therapeutic targets for these infections.

1. Introduction

Hand, foot and mouth disease (HFMD), a common viral illness among infants and children younger than 5 years old, has clinical manifestations of fever, sore throat, general malaise and vesicular rash on the hands and feet as well as exanthema on oral mucosa and tongue (Aswathyraj et al., 2016). HFMD is mostly caused by coxsackievirus A16 (CA16) and enterovirus 71 (EV71) infection (Mao et al., 2014; Solomon et al., 2010). Although HFMD is generally asymptomatic or presents with benign symptoms, it may also lead to severe neurological complications, such as acute flaccid paralysis, encephalitis, encephalomyelitis and fulminant neurogenic pulmonary oedema, which are associated with high mortality (Muehlenbachs et al., 2015). Therefore, HFMD has emerged as a major public health problem, particularly in the Asia-Pacific region (Koh et al., 2016). In the past several years, large outbreaks of HFMD have been reported, and these were caused by the co-circulation or alternative cycling of EV71 and CA16 in China (Liu et al., 2014). Although both EV71 and CA16 belong to the human enterovirus A (HEV-A) species of the Picornaviridae family, the clinical manifestations and pathogenesis of HFMD caused by the two viruses have some discrepancies (Li et al., 2011; Puenpa et al., 2011). Generally, EV71 infection easily progresses into serious central nervous system (CNS) complications and even leads to death, while CA16 infection often results in mild and self-limited clinical symptoms (Mao et al., 2014; Solomon et al., 2010). In consideration of the con-

* Corresponding author at: Institute of Medical Biology, Chinese Academy of Medical Science and Peking Union Medical College. 935 Jiaoling Road, Kunming, Yunnan, China.
E-mail address: liqihan@imbcams.com.cn (Q. Li).

http://dx.doi.org/10.1016/j.virusres.2016.11.024

spicuous morbidity and mortality induced by EV71 infection, the development of a HFMD vaccine has mainly targeted EV71 in recent years. Also, an inactivated EV71 vaccine has successfully entered into the market, but this vaccine does not provide effective protection against infections with other enteroviruses, such as CA16 (Li et al., 2014a; Li et al., 2014b). Additionally, accumulating evidence has revealed that a small number of patients infected with CA16 are also capable of developing potentially severe neurological complications, such as aseptic meningitis, encephalitis and even fatal neurogenic pulmonary oedema, which can elicit serious injury or even death (Mao et al., 2014). Thus, on-going explorations into the molecular bases of HFMD pathogenesis and progression caused by EV71 and CA16 infection may reveal novel approaches for the development of a CA16 monovalent vaccine or an EV71-CA16 bivalent vaccine, improving the prophylaxis and treatment of HFMD and potentially even eradicating the disease.

microRNAs (miRNAs) are short (~21 nucleotides long), endogenous, non-coding RNAs (Krol et al., 2010; Treiber et al., 2012). Their discovery has greatly expanded our understanding of the cellular mechanisms that regulate gene expression by the sequence-selective targeting of messenger RNAs (mRNAs), leading to their cleavage or reduction in the translational efficiency (Ha and Kim, 2014). Furthermore, miRNA biogenesis has unique tissue-specific, developmental stage-specific and disease-specific patterns (Winter et al., 2009). Recently, an increasing number of studies have demonstrated that miRNAs govern a wide variety of biological processes, such as the establishment and maintenance of the cell fate of immune cells, the regulation of innate immune and adaptive immune responses, the modulation of tissue differentiation, cellular apoptosis, signal transduction and organ development (Lee et al., 2014; O'Connell et al., 2010). Moreover, miRNA dysregulation is associated with many diseases, including cancer, neuro-developmental disorders, cardiovascular disorders and most inflammatory diseases (Busch et al., 2016; Mehta and Baltimore, 2016; Piva et al., 2013). As such, miRNAs are increasingly recognized as biomarkers for disease diagnosis as well as novel therapeutic targets (Busch et al., 2016; Louten et al., 2015). As understanding of miRNAs has increased in recent decades, it has been revealed that miRNAs of cellular origin are likely involved in cellular defences against viral infections, whereas miRNAs of viral origin might confer multiple defences to enhance viral replication and survival in host cells (Cullen, 2006; Skalsky and Cullen, 2010; Sullivan and Ganem, 2005). Therefore, research into cellular and virus-encoded miRNA function will not only augment our understanding of host-virus interplay but also reveal new approaches for the treatment of virus-induced diseases.

Currently, accumulating evidence has indicated that EV71 infection can elicit ectopic miRNA expression, resulting in cellular apoptosis, which is an important cellular defence mechanism, particularly in the early phase of pathogen infection (Ho et al., 2016; Wu et al., 2015). Moreover, many studies have clearly shown that the miRNAs that are induced by EV71 infection can directly target host genes, leading to cellular or tissue malfunctions and viral pathogenesis (Lei et al., 2016; Wu et al., 2015). Hence, based on the above studies and the different clinical symptoms that are produced by EV71 and CA16 infection, we hypothesized that the host miRNAs induced by CA16 infection might be distinct from those induced by EV71 infection. Alternatively, EV71 and CA16 infection both triggered some of the same miRNAs, but their expression levels may present opposite between the two viruses. Additionally, our previous study demonstrated that EV71 infection presented more typical pathologic changes in the respiratory tract than in the alimentary tract (unpublished results). However, it has become increasingly clear that airway epithelial cells are not only central participants in defending against foreign pathogens by producing dozens of antimicrobial molecules but also regulate both innate and adaptive immunity through recruiting immune system cells, including dendritic cells (DCs), T cells and B cells (Brune et al., 2015; Kato and Schleimer, 2007). Moreover, our previous work confirmed that EV71 and CA16 can be captured by different subsets of DCs in airway epithelial cells in EV71 and CA16 airway-infected infant rhesus monkeys (unpublished results). Therefore, we hypothesized that differences generated in the respiratory tract following infection with these two viruses could lead to variations in the immune responses to or pathogenesis induced by the viruses. Subsequently, high-throughput sequencing was used to detect differences in human bronchial epithelial (16HBE) cells, a pivotal target of enterovirus infection within the respiratory tract, following EV71 or CA16 infection.

2. Materials and methods

2.1. Cell culture and virus infection

16HBE cells purchased from the Jennino Biological Technology were maintained in RPMI 1640 (Gibco, USA) supplemented with L-glutamine, penicillin, streptomycin and 10% fetal bovine serum (FBS, Gibco, USA) at 37 °C in a 5% CO_2 containing incubator. For in vitro virus infection, approximately 1×10^5 16HBE cells per well were plated in 6-well plates and incubated overnight at 37 °C under 5% CO_2. The 16HBE cells grown to 80% confluence and infected with EV71 (sub-genotype C4, GenBank: EU812515.1) or CA16-G20 strain (sub-genotype B, GenBank: JN590244.1), which were isolated from an epidemic in Fuyang, China in 2008 and from an HFMD patient in Guangxi, China in 2010, respectively. The cells were infected at a multiplicity of infection (MOI) of 10. The cells were harvested at 0, 6 and 12 h post infection (hpi). Cells infected with EV71 and CA16 for 0 hpi were used as controls. Simultaneously, we defined the following experimental groups: EV71–0 h, EV71–6 h, EV71–12 h, CA16–0 h, CA16–6 h and CA16–12 h. Additionally, the EV71–0 h and CA16–0 h were used for normalization (the normalization value was set to 1), and these two groups were designated the Con. Each group was evaluated in triplicate and pooled separately for subsequent total RNA extraction.

2.2. RNA isolation and quality control

Samples from the above groups were sent to the National Engineering Center for Biochips in Shanghai. miRNA was extracted from each group of cells using a mirVana™ miRNA Isolation Kit (Ambion, USA) according to the manufacturer's instructions. RNA was further purified using a miRNeasy Mini kit (Qiagen, Germany) following the manufacturer's protocol. RNA concentration and RNA integrity were assessed by capillary electrophoresis on an Agilent 2100 Bioanalyzer (Agilent Technologies, USA); only samples with an RNA integrity number (RIN) > 7 were used for miRNA profile analysis.

2.3. Small RNA library preparation, high-throughput sequencing and miRNA-seq data analysis

High-throughput sequencing is a useful tool for transcriptome studies, as it can capture almost all expressed transcripts, including known and novel transcripts. Additionally, it has lower background noise and higher sensitivity than microarrays (Chen et al., 2011). Sequencing libraries of the above samples were generated using a standard TruSeq Small RNA sample preparation kit (Illumina, USA) according to manufacturer recommendations and then prepared for Illumina sequencing. Low-quality sequences, namely, those with undetermined nucleotides (Ns), a quality score (Q-score) less than 10, or reads shorter than 18 nt, were filtered from the libraries. The adapter sequences were also removed. Clean reads for small RNAs (sRNAs) were acquired and mapped using Rfam

(http://rfam.janelia.org/) and piRNA (http://pirnabank.ibab.ac.in/) to remove non-coding RNAs (e.g., rRNA, tRNA, snoRNA, or snRNA) and repetitive RNAs. After the sRNAs were filtered with the above-mentioned processes and excluded, the remaining short reads were mapped to the known miRNA precursors, and the mature miRNAs were deposited in miRBase 19.0 (available online: http://www.mirbase.org/). Unmappable sequences were used to predict potentially novel candidate miRNAs with the Mfold RNA folding prediction web server (available online: http://mfold.rna.albany.edu/). Finally, 18–35 nt lengths of known and novel miRNAs were selected for further analysis. The sequencing data were deposited in the National Center for Biotechnology Information's Gene Expression Omnibus (GEO) database (www.ncbi.nlm.nih.gov/geo/) under accession number GSE85829.

2.4. Data analysis

2.4.1. Principal component analysis (PCA)

Clean data were obtained from the pre-processed miRNAs-seq data and then submitted to PCA to determine similarities and discriminations among the groups.

2.4.2. Differential expression analysis of miRNA sequences

To compare differential miRNA expression among the above-described groups, miRNA frequency was normalized to the number of transcripts per million clean tags (TPM). Subsequently, a fold change ≥ 2 indicated that the miRNAs in the EV71- and CA16-infected samples were up-regulated, while a fold change ≤ 0.5 indicated that the miRNAs in the EV71- and CA16-infected samples were down-regulated. A P-value < 0.05 was selected as the cut-off criterion.

2.4.3. Clustering analysis

Hierarchical clustering, a method of non-monitoring cluster analysis, was used to achieve the clustering of the different miRNAs and groups of samples, enabling detection of the differential expression patterns of the miRNAs in the different groups. This was accomplished using average linkage clustering with Euclidean distances, treating the samples independently of each other, with the gplots heatmap.2 function of the R program. The normalized data were transformed to a log 2 scale for visualization purposes.

2.4.4. Trend analysis

Log standardization of the differentially expressed miRNAs was performed to facilitate trend analysis of the miRNA expression changes in the different groups.

2.4.5. Target prediction and functional enrichment of differentially expressed miRNAs

Target genes of the differentially expressed miRNAs isolated by trend analysis were predicted using the TargetScan (Lewis et al., 2003) and miRDB prediction programs (Wong and Wang, 2015). We defined putative targets by using the top 200 genes in TargetScan and a target score ≥ 80 in miRDB. To increase the reliability of the results, only target genes identified by both databases were considered to be predicted target genes for the differentially expressed miRNAs. Significantly enriched GO categories were determined based on the false discovery rate (FDR ≤ 0.05). The FDR was calculated based on the Benjamini–Hochberg method and evaluated using default parameters to adjust the p-values. In addition, the predicted miRNA target genes were analysed in terms of Kyoto Encyclopedia of Genes and Genomes (KEGG) pathways using the PANTHER Classification System.

2.4.6. Construction of regulatory networks

We constructed four regulatory networks: one containing transcription factors (TFs) and miRNAs, one containing miRNAs and target genes, one containing miRNAs and GO-biological processes, and one containing miRNAs and pathways. A complex regulatory network was generated by computational methods and aimed to reveal the crucial functions of the included miRNAs. Ensembl online tools were employed to predict the TFs of the miRNAs. Furthermore, to avoid false positives, a relative score of ≥ 0.99 was chosen to identify potential TFs. Three other regulatory networks were constructed to reveal the roles of the miRNAs based on interactions between selected differentially expressed miRNAs and their target genes, interactions between the target genes and GO-biological processes, and interactions between the target genes and pathways.

2.4.7. Hierarchical GO category analysis of deregulated miRNA-associated target genes with key GO-biological process categories

GO category trees were hierarchically created using the Gene Ontology Enrichment Analysis Software Toolkit (GOEAST) to further elucidate the critical functions of the deregulated miRNAs during EV71 and CA16 infection.

2.5. miRNA and miRNA target quantification by quantitative RT-PCR (qRT-PCR) in the validation set

To validate the sequencing data, we randomly choose 8 differentially expressed miRNAs, including 7 known miRNAs and 1 novel miRNA, for qRT-PCR analysis using a Mir-X miRNA qRT-PCR SYBR Kit (Clontech, USA). A total of 2 μg of RNA was first polyadenylated with polyA polymerase and then reverse-transcribed into cDNA with a poly(T) adapter primer under the following reaction conditions: 60 min at 37 °C, 5 min at 85 °C and maintenance at 4 °C. After this was completed, 90 μl ddH_2O was added to the cDNA for miRNA quantification. Finally, the cDNA was amplified and quantified using SYBR Advantage Premix, ROX Dye, nuclease-free water, mRQ 3′ Primer and miRNA-specific 5′ primers on a 7500 Fast Real-time PCR system (Applied Biosystems, USA) in accordance with the manufacturer's instructions. The amplification reactions were all carried out at 95 °C for 10 s, followed by 40 cycles of 95 °C for 10 s and 60 °C for 40 s and then dissociation at 95 °C for 60 s, 55 °C for 30 s and 95 °C for 30 s. U6 snRNA was served as an internal control, and the $2^{-\triangle\triangle Ct}$ method was used to evaluate relative expression. The experiment was performed using three independent biological replicates. All miRNA-specific 5′ primers used in the qPCR experiments are listed in Table S1.

Based on analysis of the predicted targets of the differentially expressed miRNAs, we randomly selected 20 targets for an indirect corroboration of miRNA expression by qRT-PCR using a 7500 Fast Real-time PCR system (Applied Biosystems, USA). Total cellular RNA was isolated with TRIzol Reagent as recommended by the manufacturer (TIANGEN, China). Reverse transcription and PCR were performed using a One Step SYBR® PrimeScript™ PLUS RT-PCR Kit (TAKARA, Japan) following the manufacturer's recommendations. The qRT-PCR cycling conditions were 1 cycle at 42 °C for 5 min and 1 cycle at 95 °C for 10 s, followed by a two-step PCR procedure consisting of 5 s at 95 °C and 34 s at 60 °C for 40 cycles. β-actin mRNA was used as an endogenous control for data normalization. All gene primers are listed in Table S2. The relative amount of expressed mRNA was also calculated by the $2^{-\triangle\triangle Ct}$ method, and the experiment was performed in technical triplicate.

Table 1
Overview of miRNA-seq data processing of all samples.

Samples	Raw reads	Clean reads	Adapter-trimmed reads (length > = 18nt)	Reads aligned to known Homo sapiens pre-miRNA in miRBase 19
EV71-0h	26,524,581	26,085,971	23,344,423	470,119
EV71-6h	23,917,420	23,594,094	21,513,316	727,081
EV71-12h	25,113,444	24,916,349	24,087,092	785,630
CA16-0h	22,778,666	22,626,697	21,930,664	523,108
CA16-6h	23,781,314	23,550,267	22,860,825	657,904
CA16-12h	18,535,354	18,212,558	16,088,596	468,647

Indicated from left to right are the numbers of reads that raw sequencing data, passed quality filtering (clean reads), the numbers of reads that passed both quality filtering, adapter filtering and length filtering (adapter-trimmed reads ≥ 18nt), and the number of reads that could be aligned to known Homo sapiens pre-miRNA in miRBase 19 with perfect matches, respectively.

2.6. Statistical analysis

For the sequencing data, the raw reads obtained from each library were normalized to TPM. For qRT-PCR, the data are expressed as the mean ± standard error means (SEM). Statistical analysis was performed using SPSS 18.0 (IBM SPSS, USA). $P < 0.05$ was considered statistically significant for all analysis.

3. Results

3.1. Overview of miRNA sequencing data in 16HBE cells infected with EV71 and CA16

To evaluate the effects of EV71 and CA16 infection on 16HBE miRNA expression, we carried out high-throughput small RNA sequencing using an Illumina platform and constructed 6 small RNA libraries. The details of the small RNA sequencing data generation for the 6 libraries and the subsequent analysis are shown in Table 1. Different types of sRNAs, including miRNA, miscellaneous RNA (misc_RNA), ribosomal RNA (rRNA), small nucleolar RNA (snoRNA), small nuclear RNA (snRNA) and others, were identified in the samples (see Fig. S1 in the online version at DOI: http://dx.doi.org/10.1016/j.virusres.2016.11.024). The read classification indicated that miRNAs presented dynamic changes in both the EV71- and CA16-infected samples, with the abundance of miRNAs in each sample being 22 nt in size. Thereafter, the discrete degree of each sample group was examined using PCA (Fig. 1a). The results revealed the distribution and clustering of the individual group samples. The Con group and infected groups formed a tight separate cluster, whereas the EV71-infected groups and the CA16-infected groups were grouped closely together, respectively. Interestingly, the CA16–6 h group was closely grouped with the EV71-infected groups. These results indicate that there was a notable disparity between the EV71-infected groups and the CA16–12 h group, whereas similarity existed between the EV71-infected groups and the CA16–6 h group.

3.2. Differential miRNA expression patterns in the EV71- and CA16-infected groups

To investigate the changes of miRNA expression profiles in the 16HBE cells during EV71 and CA16 infection, global cellular miRNA expression patterns following infection were compared with those of the controls. In this study, only those differentially expressed miRNAs with a P value < 0.05 and a fold change ≥ 2 or ≤ 0.5 are described. The results showed that, compared with the EV71–0 h group, there were 14 up-regulated and 45 down-regulated known miRNAs and 112 up-regulated and 35 down-regulated novel miRNAs in the EV71–6 h group, as well as 19 up-regulated and 65 down-regulated known miRNAs and 33 up-regulated and 50 down-regulated novel miRNAs in the EV71–12 h group. Moreover, there were 16 up-regulated and 41 down-regulated known miRNAs and 61 up-regulated and 342 down-regulated novel miRNAs in the CA16–6 h group, as well as 36 up-regulated and 42 down-regulated known miRNAs and 37 up-regulated and 34 down-regulated novel miRNAs in the CA16–12 h group relative to the CA16–0 h group (Table S3).

Subsequently, the data for all the differentially expressed miRNAs were also graphed into a Venn diagram (Fig. 1b and d). Common and distinct differentially expressed known and novel microRNAs in response to EV71 and CA16 infection across all time points were revealed. Subsequently, 154 known and 47 novel differentially expressed miRNAs were submitted to unsupervised hierarchical clustering to construct two heat maps based on the differential expression patterns with log 2 values (infected/control) and fold changes (Fig. 1c and d). A positive log 2 value indicated up-regulation, and a negative log 2 value indicated down-regulation. It is noteworthy that although 228 novel differentially expressed miRNAs were identified across the samples, only 47 novel differentially expressed miRNAs were utilized in cluster analysis, while the other 181 novel differentially expressed miRNAs were excluded. This was mainly due to a lack of expression of some of these 181 miRNAs in at least one group. In both the known and novel miRNA expression patterns, we found that the patterns induced by EV71 differed from those induced by CA16 at 6 hpi and 12 hpi. In addition, the miRNA expression patterns induced by EV71 at 6 hpi also differed from those induced by EV71 at 12 hpi, and the same was true for CA16. Therefore, these results elucidated that known and novel miRNA expression patterns following infection with EV71 and CA16 are strain- and time-specific.

Ultimately, the high-throughput dataset results were validated by performing qRT-PCR for 8 randomly selected significantly differentially expressed miRNAs, namely, miR-378c, miR-451a, miR-629-3p, miR-1287-5p, miR-3182, miR-4485-5p, miR-3651 and a novel miRNA (AGACGAGGGCTCCATAGCTC). The results were in accordance with the high-throughput dataset (see Fig. S2 in the online version at DOI: http://dx.doi.org/10.1016/j.virusres.2016.11.024).

3.3. Trend analysis of the differentially expressed miRNAs

Trend analysis of miRNA expression dynamics was used to profile the differentially expressed miRNAs and to identify the most probable set of clusters generated in the time series. As a result, we observed that 58 known and 7 novel differentially expressed miRNAs were the most significant miRNAs because their expression levels presented an opposite relationship over time following EV71 and CA16 infection, which indirectly indicates that the different manifestations that result from EV71 and CA16 infection may be closely linked to these differentially expressed miRNAs (Fig. 2a and b). In addition, the predicted structures of 7 novel differentially expressed miRNAs are displayed in Fig. 2c. For each differentially expressed miRNA, if the two ratios (EV71–6 h/CA16–6 h and EV71–12 h/CA16–12 h) fell between 0.5 and 2, the miRNA was elim-

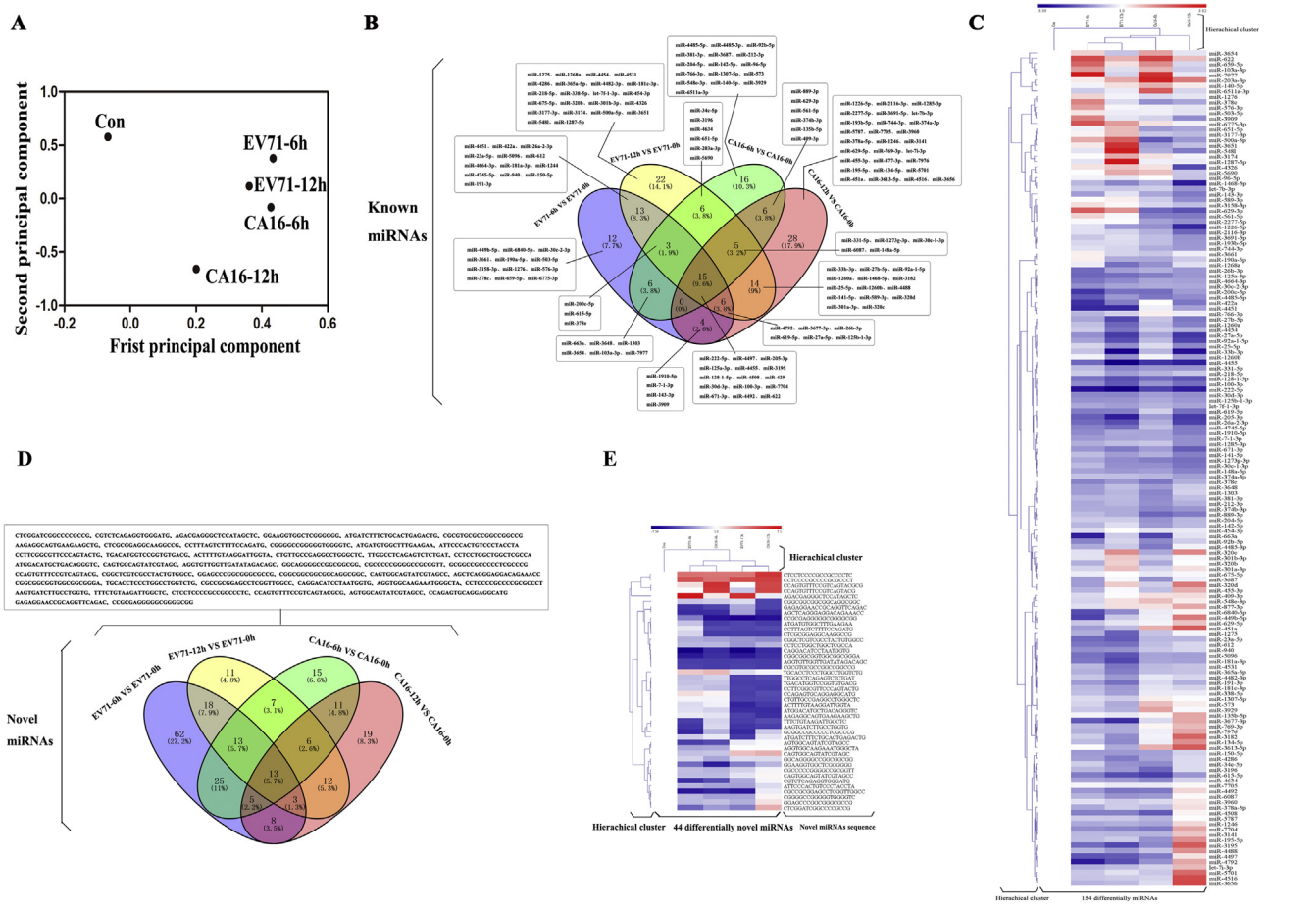

Fig. 1. Overview of all miRNAs. (a) Principal component analysis (PCA) showing the distribution and clustering of the individual sample groups. Each spot represents a single array. It exhibits a clear separation between Con group and infected groups. (b) Venn diagram representing Known differentially expressed miRNAs. (c) Time- and strain-specific regulation of differential miRNAs during EV71 and CA16 infections. The columns correspond to expression patterns of differentially expressed miRNAs during the EV71 and CA16 infections relative to Con samples at 6 hpi and 12 hpi. Significance was determined using a fold-change threshold of at least 2 and a P value cutoff of 0.05. The intensity of the miRNA expression is indicated in green (lower level of expression) and red (higher level of expression). Dendrograms between samples and between miRNAs are depicted, where the closest branches of the tree represents samples/miRNAs with the most similar expression pattern. (d) Novel differentially expressed miRNAs. The names of these miRNAs are given in boxes. (e) Venn diagram representing novel significant differentially expressed miRNAs in all samples. Colors indicate the log2 fold changes with a ratio of EV71/CA16-infected sample versus control according to the TPM. The red color represents up-regulation, while the blue color indicates down-regulation. (For interpretation of the references to colour in this figure legend, the reader is referred to the web version of this article.)

inated, leaving a total of 56 known differentially expressed miRNAs for further analysis (Table 2).

3.4. Prediction and annotation of miRNA putative target genes

To gain insight into the possible regulatory roles of the 56 known differentially expressed miRNAs during EV71 and CA16 infection, we used the TargetScan and miRDB programs to predict the potential targets of these differentially expressed miRNAs. It was found that 7417 genes were predicated to be potential targets with TargetScan, whereas 4444 genes were predicated to be potential targets with miRDB. We then looked for intersections of these genes for subsequent GO and pathway analysis. Predicted target functions were classified into biological process, molecular function, and cellular component by GO enrichment analysis based on a cut-off value of a 5% error rate ($P < 0.05$, determined by *t*-test with Benjamini–Hochberg multiple testing correction). The biological processes for the miRNA targets included biological adhesion, biological regulation, cell adhesion, cell communication, cell-cell adhesion, cellular process, developmental process, ectoderm development, nervous system development, regulation of biological process, regulation of catalytic activity, regulation of molecular function, regulation of nucleobase-containing compound metabolic process, regulation of transcription from RNA polymerase II promoter, sensory perception of chemical stimulus, system development, transcription from RNA polymerase II promoter and transcription, DNA-dependent (Fig. 3a). The molecular functions of the predicted miRNA targets included DNA binding, binding, calcium ion binding, enzyme regulator activity, nucleic acid binding transcription factor activity, protein binding and sequence-specific DNA binding transcription factor activity (Fig. 3b). Additionally, the actin cytoskeleton was a unique cellular component of the miRNA targets (Fig. 3c). Afterwards, the predicted targets genes were subjected to KEGG pathway enrichment analysis using the PANTHER Classification System. As illustrated in Fig. 4, 123 pathways were identified, suggesting that these signalling pathways are regulated by the differentially expressed miRNAs during virus infection. Furthermore, among the 123 pathways, there were 3 key pathways, namely, the Cadherin signalling pathway, the Wnt signalling pathway and angiogenesis, which had significant differences when using Bonferroni correction for multiple testing (*P* values of 0.05).

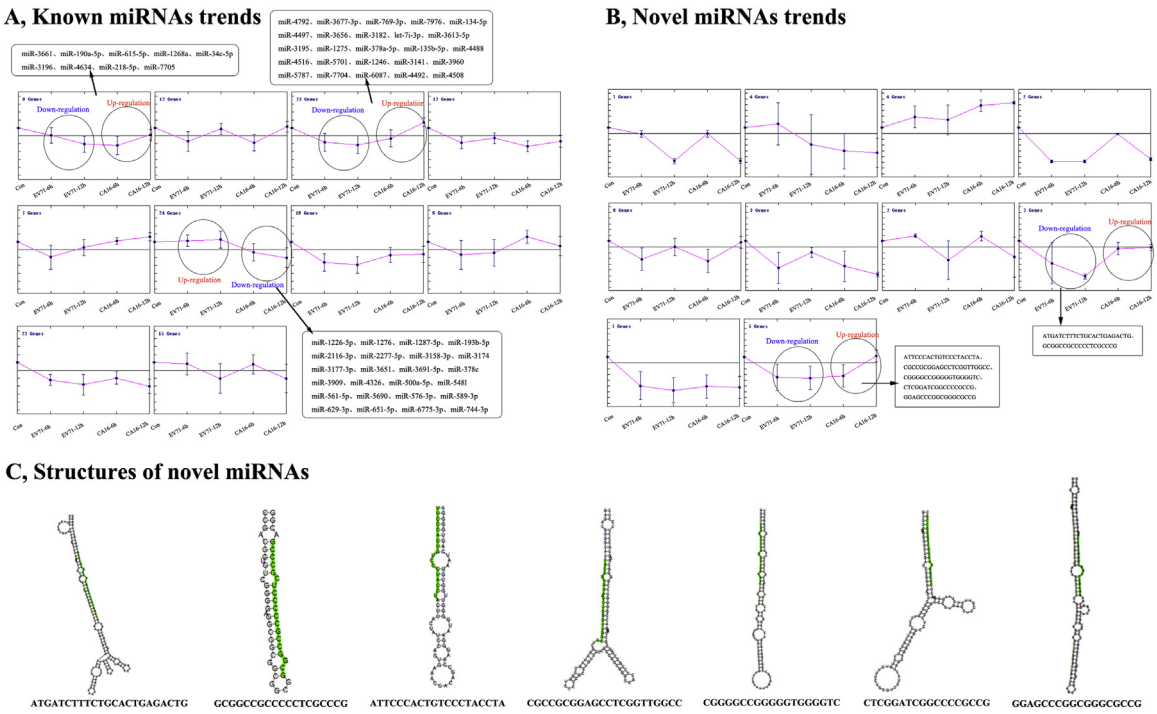

Fig. 2. Trend analysis of differentially expressed miRNAs in response to EV71 and CA16 infection over time. (a) The known differentially expressed miRNAs that showed opposite expression patterns during the progression of EV71 and CA16 infection are given in boxes. (b) The boxes display the miRNA sequences of novel differentially expressed miRNAs, which present an inverse expression between EV71 and CA16 infection. (c) The location and putative folding structure of these opposed expressed novel miRNA precursors in human. The mature miRNA is highlighted (green) in stem-loop structures obtained using Mfold. (For interpretation of the references to colour in this figure legend, the reader is referred to the web version of this article.)

3.5. miRNA-gene, miRNA-GO, miRNA-pathway and TF-miRNA regulation network construction

Building miRNA regulatory networks is very important for high-throughput analysis of interactions among miRNAs and genes, GOs, and pathways. First, to further confirm the key target genes, we looked for intersections of related genes in our GO and pathway analysis results. A total of 279 target genes were identified and listed in Fig. S3 in the online version at DOI: http://dx.doi.org/10.1016/j.virusres.2016.11.024. Next, 56 known differentially expressed miRNAs, 17 GOs involved in biological processes and 92 pathways were identified by refining the correlations among the 279 target genes and the miRNAs, GOs, and pathways. Consequently, a miRNA-gene network was built based on interactions between miRNAs and genes (Fig. 5a). A miRNA-GO network was established on the basis of relationships among significant GOs and genes and relationships among miRNAs and genes (Fig. 5b). A miRNA-pathway network was constructed in accordance with relationships among significant pathways and genes and relationships among miRNAs and genes (Fig. 5c). miRNAs not only mediate specific target gene products via hybridization to mRNA but are also regulated by TFs. Therefore, we performed TF-miRNA network analysis to study the relationships that existed among the potentially predicted TFs and the 56 known differentially expressed miRNAs (Fig. 5d). These regulatory networks demonstrated that the differentially expressed miRNAs might play an important role in pathogenesis following EV71 and CA16 infection.

3.6. Hierarchical GO category analysis and detection of target genes involved in key biological processes

In this part, we specifically looked into the hierarchical GO categories of the deregulated miRNA-associated target genes and the key biological processes. 16HBE cells are airway epithelial barrier cells and play an important role in airway defence, which is maintained through cell adhesion (Tam et al., 2011). Hence, we focused on GOs related to adhesion and identified 3 GO terms, namely, biological adhesion, cell adhesion and cell-cell adhesion in the biological process categories of the GO analysis. In total, 47 target genes were identified among these 3 GO terms, and their corresponding 24 known differentially expressed miRNAs are listed in Table S4. Of these 24 miRNAs, 17 miRNAs were overexpressed and 7 miRNAs were reduced in the EV71 samples, while 17 miRNAs were decreased and 7 miRNAs were increased in the CA16 samples. These target genes were then submitted to hierarchical GO category analysis. In Fig. 6, the white circles represent the miRNAs of no significance and the yellow circles represent the miRNAs that were significantly overrepresented in the 21 biological processes (P value < 0.05).

Eventually, we randomly selected 12 of the 47 target genes for further analysis to confirm the miRNA sequencing data. The expression levels of the miRNAs and their targets generally presented opposite interactions based on the regulatory mechanisms of the miRNAs. Except for LEF1 and NTNG1, the expression levels of the other genes were inversely correlated with miRNA expression (see Fig. S4 in the online version at DOI: http://dx.doi.org/10.1016/j.virusres.2016.11.024).

4. Discussion

EV71 and CA16 have still been recognized as a major etiological agent responsible for HFMD epidemics, which seriously inflicts children worldwide (Koh et al., 2016). The development of an inactivated EV71 vaccine has substantially improved the health of children both in China and worldwide. However, this vaccine fails to elicit protection against CA16 infection (Li et al., 2014a; Li et al., 2014b). Thus, further investigations identifying the factors that cause the different manifestations of EV17 and

Table 2
Oppositely expressed miRNAs during the course of EV71 and CA16 infection.

miRNAs	EV71–6 h (FC)	CA16-6 h (FC)	Ratio (EV71-6 h/CA16-6 h)	EV71-12 h (FC)	CA16-12 h (FC)	Ratio (EV71-12 h/CA16-12 h)
miR-1268a	1.551802	0.397556	3.903349	0.239359	1.302244	0.183805
miR-190a-5p	2.198386	0.567938	3.870821	0.598397	0.956751	0.625448
miR-218-5p	**0.969876**	**0.681525**	**1.423096**	**0.489598**	**0.903598**	**0.541832**
miR-3196	0.711242	0.198778	3.57807	0.448798	1.209226	0.371145
miR-34c-5p	1.010288	0.366975	2.753013	0.411398	1.202071	0.342241
miR-3661	2.198386	0.883459	2.488385	1.077115	1.612302	0.668061
miR-4634	0.52133	0.32907	1.584252	0.454803	1.041951	0.436492
miR-615-5p	0.287371	0.099389	2.89137	0.132977	0.418578	0.317688
miR-7705	**1.755014**	**1.490837**	**1.177201**	**1.453251**	**2.092892**	**0.694375**
let-7i-3p	0.646584	1.060151	0.609898	0.769368	2.976557	0.258476
miR-1246	0.577015	0.564645	1.021907	0.647633	2.507426	0.258286
miR-1275	0.618472	0.864253	0.715614	0.182121	1.74711	0.104241
miR-134-5p	0.775901	1.590226	0.487919	0.359038	3.906732	0.091903
miR-135b-5p	1.697283	2.120301	0.800492	1.421194	3.348627	0.424411
miR-3141	0.727407	0.695724	1.04554	0.710597	2.790523	0.254647
miR-3182	0.97309	1.684882	0.577542	0.377121	5.244411	0.071909
miR-3195	0.2176	0.346588	0.627837	0.12083	5.552424	0.021762
miR-3613-5p	1.939752	3.180452	0.609898	0.598397	5.581045	0.10722
miR-3656	0.683085	1.209955	0.564554	0.757648	6.503131	0.116505
miR-3677-3p	0.161646	1.192669	0.135533	0.0748	3.348627	0.022337
miR-378a-5p	0.579696	0.773026	0.749905	0.980134	2.418453	0.405273
miR-3960	1.293168	1.169284	1.105949	0.957436	2.298077	0.416625
miR-4488	0.683887	0.841884	0.812329	0.448798	3.873902	0.115852
miR-4492	0.44592	0.270038	1.651321	0.254491	2.527266	0.100698
miR-4497	0.146951	0.280628	0.52365	0.163199	2.363737	0.069043
miR-4508	0.303397	0.164208	1.847638	0.308405	2.135356	0.144428
miR-4516	0.880349	1.073403	0.820148	0.94823	6.306581	0.150356
miR-4792	0.052235	0.397556	0.131391	0.132977	3.348627	0.039711
miR-5701	0.905218	0.905218	1	1.316474	5.022941	0.262092
miR-5787	0.952942	0.696479	1.368228	0.936065	2.040261	0.458797
miR-6087	0.679484	0.458719	1.481264	0.421302	2.071426	0.203387
miR-769-3p	0.727407	2.120301	0.343068	0.598397	2.976557	0.201037
miR-7704	0.383161	0.274946	1.393588	0.332443	3.404264	0.097655
miR-7976	0.646584	1.590226	0.406599	0.598397	3.348627	0.178699
miR-1226-5p	1.293168	0.397556	3.252791	0.470119	0.065389	7.189628
miR-1276	2.586336	1.192669	2.168527	1.675513	1.395261	1.20086
miR-1287-5p	1.375363	1.590226	0.864885	11.45577	1.488279	7.697332
miR-193b-5p	1.131522	0.795113	1.423096	1.196795	0.446484	2.68049
miR-2116-3p	1.293168	0.650547	1.987817	1.077115	0.202947	5.307371
miR-2277-5p	1.810435	0.511144	3.541928	1.914872	0.398646	4.803438
miR-3158-3p	2.42469	1.135876	2.134644	2.094391	0.797292	2.62688
miR-3174	1.939752	2.385339	0.813198	3.291186	1.674314	1.965693
miR-3177-3p	2.15528	0.883459	2.439593	2.991987	0.744139	4.020735
miR-3651	2.263044	0.505981	4.472588	7.779167	0.811788	9.582753
miR-3691-5p	0.889053	0.795113	1.118147	1.271595	0.418578	3.037889
miR-378c	4.202797	0.397556	10.57157	1.196795	0.558105	2.144392
miR-3909	4.310561	1.060151	4.065989	1.396261	0.37207	3.752686
miR-4326	2.370808	2.385339	0.993908	2.792522	0.118501	23.56537
miR-500a-5p	3.23292	0.159023	20.32994	5.385577	0.446484	12.06221
miR-548l	1.375363	0.596335	2.30636	10.18291	0.279052	36.49105
miR-561-5p	2.586336	0.298167	8.674109	1.795192	0.279052	6.433177
miR-5690	1.939752	2.862407	0.677665	3.291186	0.892967	3.685674
miR-576-3p	3.556212	1.590226	2.236294	1.795192	1.395261	1.286635
miR-589-3p	2.047516	0.954136	2.145939	2.194124	0.37207	5.897079
miR-629-3p	5.50145	0.198778	27.67632	3.818591	0.139526	27.36829
miR-651-5p	1.61646	0.463816	3.485133	2.991987	0.558105	5.36098

Two miRNAs eliminated are given in bold. FC, fold change.

CA16 infection are still urgently needed and may provide new strategies for the development of more efficacious vaccines to prevent HFMD outbreaks. In the current study, we identified a total of 154 known and 47 novel differentially expressed miRNAs across different time points following EV71 and CA16 infection, indicating that miRNA expression has strain- and time-specific tendencies in the context of these viruses. Cellular miRNAs, which regulate over 60% of all human genes through the degradation of target mRNAs or the suppression of mRNA translation following specific binding to target mRNA, affect a multitude of cellular process, and their deregulation has been associated with the development and progression of various diseases (Treiber et al., 2012). Moreover, emerging evidence has shown that miRNAs regulate cross-talk between host and pathogen in viral infections, which is a major component of viral pathogenesis (Cullen, 2006; Skalsky and Cullen, 2010). For example, hepatitis C virus (HCV) notably increases cellular miRNA-122 expression, which in turn activates viral genomic RNA replication, resulting in pathogenic processes and regulating host anti-apoptotic gene expression to enhance viral replication (Shan et al., 2007). Additionally, a growing body of evidences have revealed that some small RNA molecules were revealed to be involved in the infectious cycle of CA16 or EV71 by different researchers, for example, elevated expression of circulating miR876-5p is a specific response to severe EV71 infections (Wang et al., 2016); EV71 could utilize host miRNAs to enhance (e.g., miRNA-548 and miRNA-146a) or suppress (e.g., miRNA-526a) its survival by directly or indirectly targeting host molecules related to immune system processes

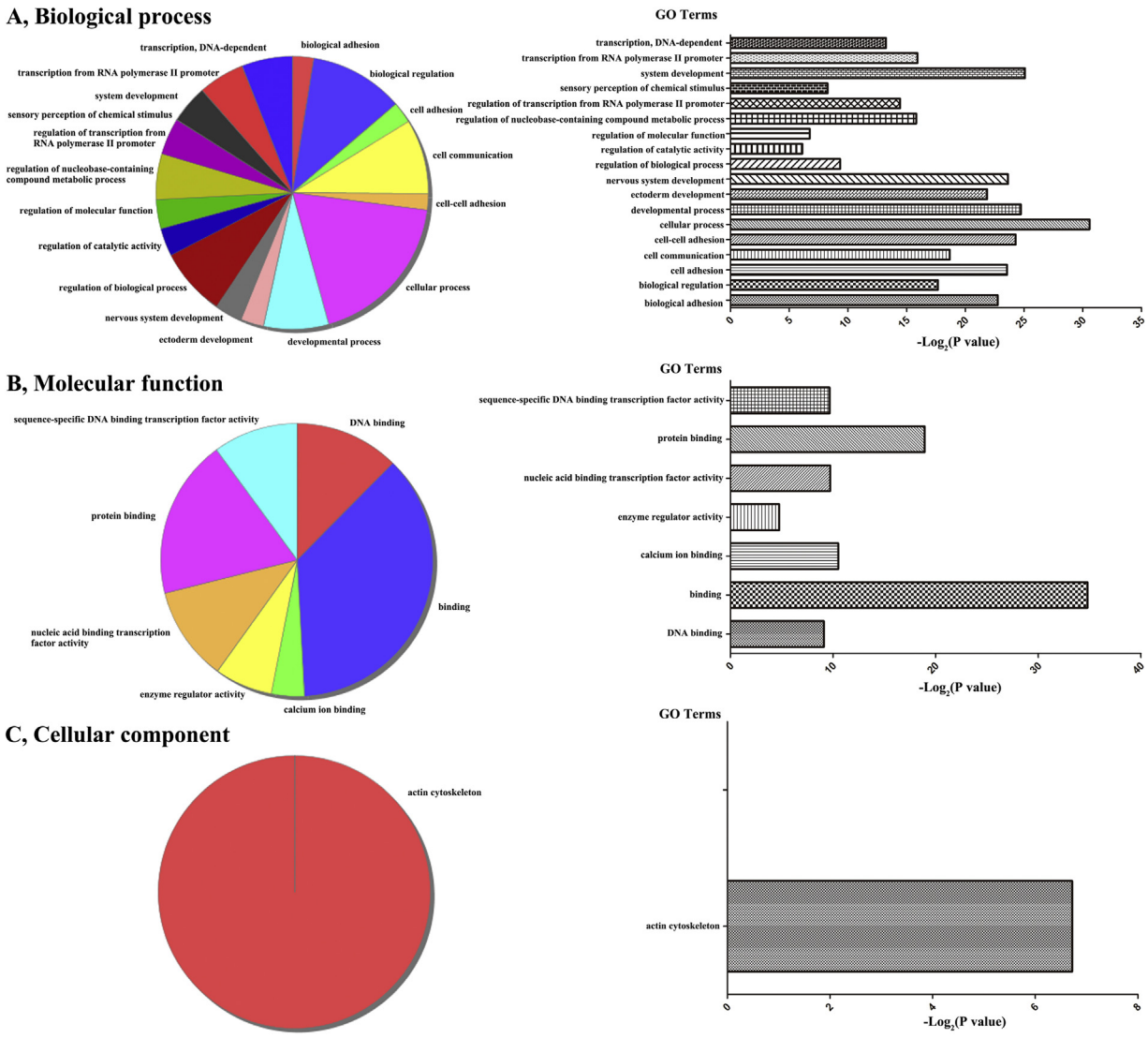

Fig. 3. Significantly enriched GO terms of biological process, molecular function and cellular component for the predicted targets. The DAVID web-based tool was used to analyze (a) biological process, (b) molecular function and (c) cellular component. GO functional enrichment annotations exhibit in pie charts of the left panel. The horizontal axis plots the negative log of the adjusted *P* value (-$\log_2 P$) and the vertical axis exhibits the GO category in bars of the right panel. (For interpretation of the references to colour in this figure legend, the reader is referred to the web version of this article.)

during infection (Wu et al., 2015); miR432* regulate the replication of CA16 in RD cells (Yang and Tien, 2014b). Furthermore, other studies have verified that host miRNA expression significantly changes in response to EV71 infection in Hep2 cells and RD cells, which also implies that altered miRNA expression might play an essential role in EV71-host interactions (Cui et al., 2010; Yang and Tien, 2014a). Nonetheless, there are few studies on systematically comparing the common and differential aspects of cellular miRNA alterations upon two enteroviral infections. Hence, our discovery of the specific miRNA expression patterns that are produced during EV71 and CA16 infection provides powerful insights into the different mechanisms of viral pathogenesis that are regulated by miRNAs. Subsequently, to further elucidate the key disparities between EV71 and CA16 infection, we further isolated 56 differentially expressed miRNAs that displayed opposite expression trends. Preliminary reports of the functions of these 56 miRNAs have been made. For instance, miRNA-1246 was discovered as a target gene of p53 in the carcinogenic process of various cancers, including cervical, colorectal, oesophageal, hepatic and pancreatic cancers (Kim et al., 2016). miRNA-3561 is closely related to tumour progression and clinical prognosis in oesophageal squamous cell cancer (ESCC) and can therefore be used as an independent prognostic biomarker for patients with ESCC (Wang et al., 2015). miRNA–548 l is involved in the migration and invasion of non-small cell lung cancer through its targeting of the AKT1 signalling pathway (Liu et al., 2015). However, the differential miRNA expression patterns in this study that follow EV71 and CA16 infection remain largely unknown and need further exploration. Recent studies have been reported that different miRNAs profiles of EV71 and CA16 infections were presented because of different infected-cells or samples. For example, our previous study on different miRNA profiles in rhesus monkey peripheral blood mononuclear cells infected with EV71 and CA16 have revealed that 20 (miR-96, let-7e-5p, miR-30a-3p, miR-582-5p, miR-204-5p, miR-19b, miR-301b, miR-19a-3p, miR-301a-3p, miR-182, miR-34c-5p, miR-200a-3p, miR-183-5p, miR-194-5p, miR-193b-3p, miR-193a-3p, miR-196a-5p, miR-196b-5p, miR-376a-3p, miR-146b-5p) known differentially expressed miRNAs involved in immune system processes are the key miRNAs that underlie the different immune responses induced by EV71 and CA16 infection (Hu et al., 2016). Cui et al. also found that three key miRNAs (miR-545, miR-324-3p, and miR-143)

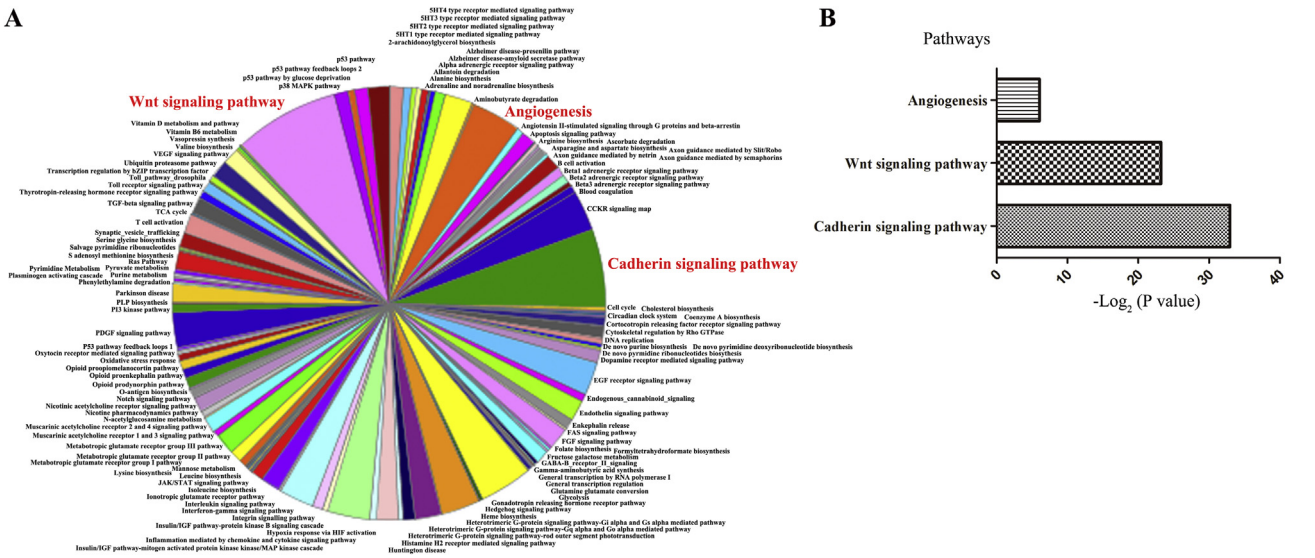

Fig. 4. KEGG terms of the predicted targets of the differentially expressed miRNAs. (a) 123 KEGG pathway annotations for the miRNAs targets are exhibited in pie chart. The red fonts represented the differential pathways. (b) 3 differential pathways were displayed by a histogram with the $-\log_2 P$ value on the X-axis. (For interpretation of the references to colour in this figure legend, the reader is referred to the web version of this article.)

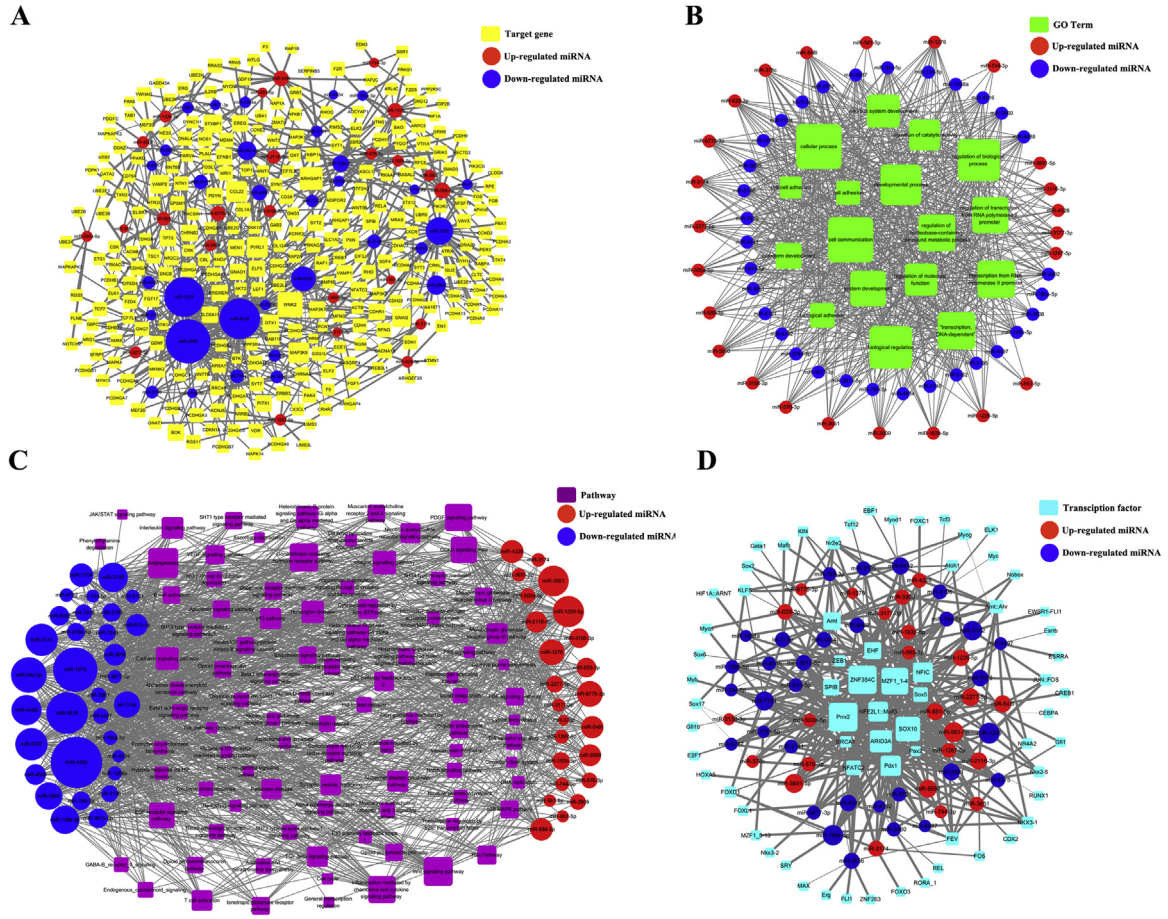

Fig. 5. Complexity of the miRNA-targets network, miRNA-GOs network, miRNA-pathways network and miRNA-TFs network after infection with EV71 and CA16. All red circles indicate upregulated miRNAs, while all dark blue circles indicate downregulated miRNAs in EV71 infection. Thus, these up-regulated and down-regulated miRNAs in EV71 infection are decreased and increased in CA16 infection, respectively. Names of all miRNAs, targets, GOs, pathways and TFs are shown in figures. The size of nodes is relative to the importance of the miRNAs and other nodes. (a) miRNA-targets network. The targets are displayed by yellow color rounded rectangles. The thickness of the edges corresponds to the free energy of miRNA-mRNA duplex. (b) miRNA-GOs network. GO term nodes are depicted as green color rounded rectangles. Edges in the network represent inhibitory effect of miRNAs on GOs. (c) miRNA-pathways network. Purple rectangle-shaped nodes denote pathways. Edges indicate a negative correlation between miRNA and pathways. (d) miRNA-TFs network. Light blue rounded rectangles represent putative TFs. The grey lines width reflects the relative score. (For interpretation of the references to colour in this figure legend, the reader is referred to the web version of this article.)

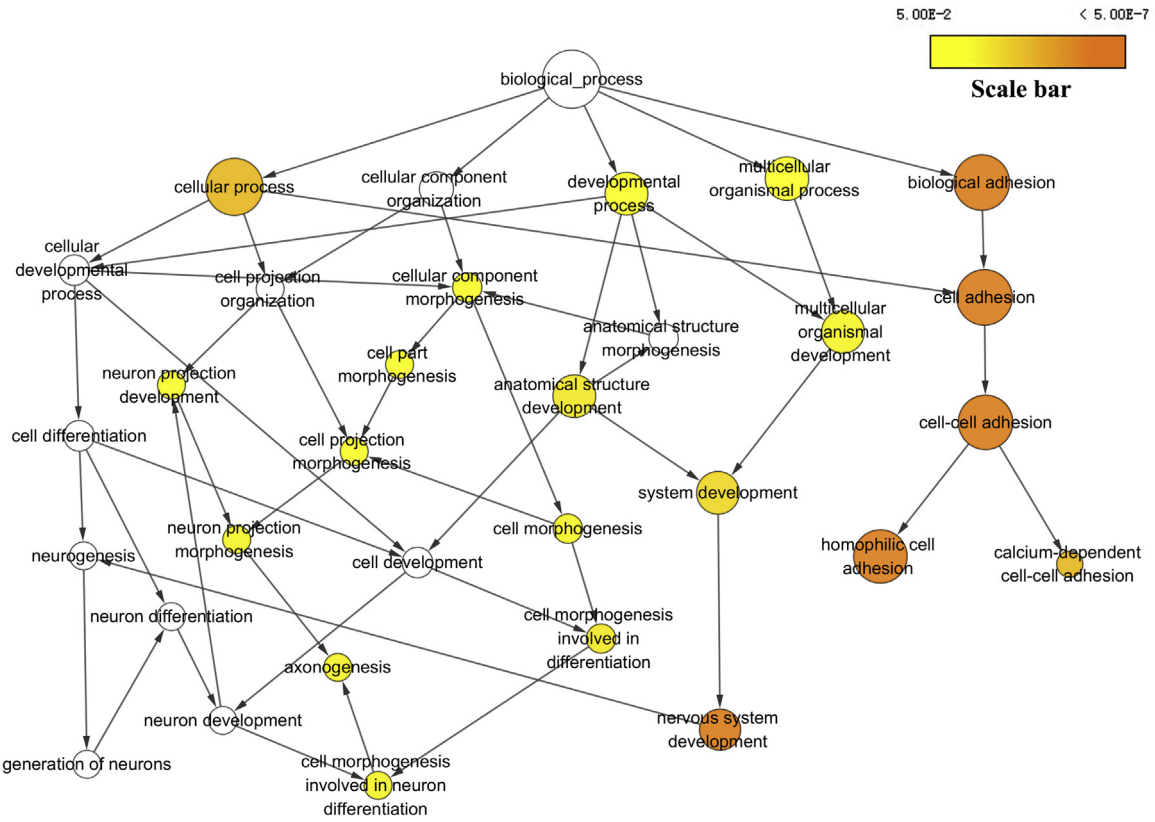

Fig. 6. Hierarchical GO categories of genes involved in adhesions. A *P* value cutoff of 0.05 was used to determine significantly enriched GOs. The color gradient of the yellow nodes, from light to dark, displays the *P* value, from high to low (the lower the *P* value, the greater the GO significance level). White nodes are no significant. (For interpretation of the references to colour in this figure legend, the reader is referred to the web version of this article.)

can be used to distinguish EV71 infection from CA16 infection in patients with HFMD and provide supplemental biomarkers for diagnosing and subtyping enteroviral HFMD infections (Cui et al., 2011). And Zhu et al. manifested that the expression levels of 15 (miR-4508, miR-638, miR-762, miR-4466, miR-4787-5p, miR-3196, miR-3960, miR-4516, miR-3656, miR-4668-5p, let-7b, miR-320d, miR-151-5p, miR-4739, miR-320e) and 5(miR-26b, miR-20b, miR-574-3p, miR-1280, miR-22) miRNAs were significantly changed in CA16- and EV71-infected cells, respectively (Zhu et al., 2016). Although the above mentioned miRNAs, as well as the 56 miRNAs in current study, from different researchers were different, target gene prediction and subsequent bioinformatic analysis of these miRNAs could give a new clue to enhance our understanding of the roles of miRNAs in HFMD pathogenesis.

To gain further insights into the miRNA-regulated mechanisms that occur during EV71 and CA16 infection, we used GO and pathway analysis of the predicted target genes of the 56 differentially expressed miRNAs that were identified in trend analysis. Using KEGG pathway analysis and GO annotation for target genes can offer a better understanding of the target genes at the pathway, molecular, cellular and biological levels. Our pathway enrichment analysis of the miRNA-predicted targets showed that the differentially expressed miRNAs were involved in many immune-related pathways, such as apoptosis signalling pathway, B cell activation, CCKR signalling map, inflammation mediated by chemokine and cytokine signalling pathway, interferon-gamma signalling pathway, interleukin signalling pathway, JAK-STAT signalling pathway, O-antigen biosynthesis, PI3 kinase pathway, Toll receptor signalling pathway, T cell activation and FAS signalling pathway. Furthermore, biochemical and genetic studies have clarified that miRNAs act as key regulators in the regulation of immune function, such as antigen presentation (e.g., miR-155), T cell receptor signalling (e.g., miR-181a), Toll-like receptor signalling and ensuing cytokine responses (e.g., miR-146), etc (Sonkoly et al., 2008). Thus, we hypothesized that miRNAs play a critical role in the regulation of immune response during EV71 and CA16 infection in this work. Additionally, the cellular component of GO analysis identified that these genes are only enriched in actin cytoskeleton. Nevertheless, invasion of pathogens into host cells largely depends on actin cytoskeleton rearrangement (Zhang et al., 2015). Hence, this result indicated that miRNAs exert a possible regulatory mechanism on genes associated with the actin cytoskeleton to influence viral invasion. Next, the associations of the identified miRNAs with target genes, GOs, pathways and TFs were further visualized by creating regulatory networks.

Airway epithelial cells form a complex physical barrier through tight cell-cell interactions and have a critical role in protecting against invading pathogens and establishing mechanical strength (Bals and Hiemstra, 2004; Brune et al., 2015). Once the integrity of the airway epithelium is disrupted, viral pathogenesis is facilitated through increased viral invasion (Ganesan et al., 2013). Thus, we mainly focused on the biological adhesion, cell adhesion and cell-cell adhesion results derived from the GO analysis to perform a more in-depth hierarchical GO category analysis. Among the 24 differentially expressed miRNAs related to biological adhesion, cell adhesion and cell-cell adhesion, 17 exhibited a trend of consistent expression, being predominantly down-regulated during EV71 infection and up-regulated during CA16 infection. Because of the negative regulation that miRNAs exert on their target genes, it was proposed that an inverse correlation existed between the miRNAs and the corresponding GOs of their target genes. Notably, the functions of biological adhesion, cell adhesion and cell-cell adhesion induced by CA16 infection were significantly inhibited, whereas they were activated by EV71 infection. These results indicate that

the biological adhesion, cell adhesion and cell-cell adhesion functions that are induced by CA16 infection are more susceptible to dysregulation than they are in the context of EV71 infection. Moreover, most of the target genes linked to biological adhesion, cell adhesion and cell-cell adhesion for the above 17 differentially expressed miRNAs were overexpressed during EV71 infection but reduced during CA16 infection, as validated by qRT-PCR. Therefore, it further demonstrated that epithelial cell-cell contacts could be disturbed during CA16 infection, indicating epithelial barrier impairment. In addition, the cadherin signalling pathway and the Wnt signalling pathway, which exhibited significant differences during EV71 and CA16 infection, are both highly related to epithelial barrier function (Schlingmann et al., 2015; van Zuylen et al., 2016).Taken together, we could hypothesize that the repeatedly occurring phenomenon of CA16 infection in clinical features could probably due to that CA16 infection easily caused destruction of 16HBE cells, which rarely happens following EV71 infection. With regard to other distinct clinical symptoms following CA16 and EV71 infection might be related to airway epithelial cell immune responses, including cytokine and chemokine release, recruitment of neutrophilic leucocytes and dendritic cells, and migration of dendritic cells to T-cell-enriched areas of draining regional lymph nodes, etc. Additionally, in our hierarchical GO category analysis, it was also discovered that some GO terms involved in the nervous system, such as neuron projection development, neuron projection morphogenesis, axongenesis and nervous system development, might underlie the discrepant neuropathological manifestations that exist between EV17 and CA16 infection.

In summary, small RNA sequencing technology and bioinformatics approaches were employed to identify miRNAs that are differentially regulated in response to EV71 and CA16 infection in 16HBE cells. The current study highlighted specific differential expression patterns of miRNAs during EV71 and CA16 infection, although the exact functions of these miRNAs in viral pathogenesis remain to be determined. GO and pathway analysis of the predicted targets of the differentially expressed miRNAs screened from trend analysis provided comprehensive information about the discrepant biological functions and pathways that are involved EV71 and CA16 infection. Furthermore, the construction of detailed regulatory networks would greatly contribute to a better understanding of the miRNA-mediated mechanisms that are involved in EV71 and CA16 infection. Consequently, it is worth noting that the 24 differentially expressed known miRNAs related to biological adhesion, cell adhesion and cell-cell adhesion that were identified in this study may be the key miRNAs involved in modulating the function of the epithelial barrier. Furthermore, the 7 novel differentially expressed miRNAs screened from the trend analysis and not analysed in this study require further investigation and will provide additional insights into host-pathogen interactions and pathogenesis.

Conflict of interest

The authors declare no conflicts of interest.

Acknowledgments

This research was supported by National Natural Sciences Foundation of China (31370192 and 81373142), Major National Science & Technology Specific Projects (2014ZX09102042), Yunnan Major Basic Research Program for Application (2013FA024), CAMS Initiative for Innovative Medicine (2016-I2M-1-019) and Yunnan Basic Research Program for Application (2014FB191).

Appendix A. Supplementary data

Supplementary data associated with this article can be found, in the online version, at http://dx.doi.org/10.1016/j.virusres.2016.11.024.

References

Aswathyraj, S., Arunkumar, G., Alidjinou, E.K., Hober, D., 2016. Hand, foot and mouth disease (HFMD): emerging epidemiology and the need for a vaccine strategy. Med. Microbiol. Immunol. (Berl.) 205 (5), 397–407.
Bals, R., Hiemstra, P.S., 2004. Innate immunity in the lung: how epithelial cells fight against respiratory pathogens. Eur. Respir. J. 23 (2), 327–333.
Brune, K., Frank, J., Schwingshackl, A., Finigan, J., Sidhaye, V.K., 2015. Pulmonary epithelial barrier function: some new players and mechanisms. Am. J. Physiol. Lung Cell. Mol. Physiol. 308 (8), L731–L745.
Busch, A., Eken, S.M., Maegdefessel, L., 2016. Prospective and therapeutic screening value of non-coding RNA as biomarkers in cardiovascular disease. Ann. Transl. Med. 4 (12), 236.
Chen, G., Wang, C., Shi, T., 2011. Overview of available methods for diverse RNA-Seq data analyses. Sci. China Life Sci. 54 (12), 1121–1128.
Cui, L., Guo, X., Qi, Y., Qi, X., Ge, Y., Shi, Z., Wu, T., Shan, J., Shan, Y., Zhu, Z., Wang, H., 2010. Identification of microRNAs involved in the host response to enterovirus 71 infection by a deep sequencing approach. J. Biomed. Biotechnol. 2010, 425939.
Cui, L., Qi, Y., Li, H., Ge, Y., Zhao, K., Qi, X., Guo, X., Shi, Z., Zhou, M., Zhu, B., Guo, Y., Li, J., Stratton, C.W., Tang, Y.W., Wang, H., 2011. Serum microRNA expression profile distinguishes enterovirus 71 and coxsackievirus 16 infections in patients with hand-foot-and-mouth disease. PLoS One 6 (11), e27071.
Cullen, B.R., 2006. Viruses and microRNAs. Nat. Genetics 38 (Suppl), S25–S30.
Ganesan, S., Comstock, A.T., Sajjan, U.S., 2013. Barrier function of airway tract epithelium. Tissue Barriers 1 (4), e24997.
Ha, M., Kim, V.N., 2014. Regulation of microRNA biogenesis. Nat. Rev. Mol. Cell Biol. 15 (8), 509–524.
Ho, B.C., Yang, P.C., Yu, S.L., 2016. MicroRNA and pathogenesis of enterovirus infection. Viruses 8 (1).
Hu, Y., Song, J., Liu, L., Li, J., Tang, B., Wang, J., Zhang, X., Zhang, Y., Wang, L., Liao, Y., He, Z., Li, Q., 2016. Different microRNA alterations contribute to diverse outcomes following EV71 and CA16 infections: insights from high-throughput sequencing in rhesus monkey peripheral blood mononuclear cells. Int. J. Biochem. Cell Biol. 81 (Pt A), 20–31.
Kato, A., Schleimer, R.P., 2007. Beyond inflammation: airway epithelial cells are at the interface of innate and adaptive immunity. Curr. Opin. Immunol. 19 (6), 711–720.
Kim, G., An, H.J., Lee, M.J., Song, J.Y., Jeong, J.Y., Lee, J.H., Jeong, H.C., 2016. Hsa-miR-1246 and hsa-miR-1290 are associated with stemness and invasiveness of non-small cell lung cancer. Lung Cancer 91, 15–22.
Koh, W.M., Bogich, T., Siegel, K., Jin, J., Chong, E.Y., Tan, C.Y., Chen, M.I., Horby, P., Cook, A.R., 2016. The epidemiology of hand, foot and mouth disease in Asia: a systematic review and analysis. Pediatr. infect. Dis. J.
Krol, J., Loedige, I., Filipowicz, W., 2010. The widespread regulation of microRNA biogenesis, function and decay. Nat. Rev. Genetics 11 (9), 597–610.
Lee, H.M., Nguyen, D.T., Lu, L.F., 2014. Progress and challenge of microRNA research in immunity. Front. Genet. 5, 178.
Lei, X., Xiao, X., Wang, J., 2016. Innate immunity evasion by enteroviruses: insights into virus-host interaction. Viruses 8 (1), pii: E22.
Lewis, B.P., Shih, I.H., Jones-Rhoades, M.W., Bartel, D.P., Burge, C.B., 2003. Prediction of mammalian microRNA targets. Cell 115 (7), 787–798.
Li, Y., Zhu, R., Qian, Y., Deng, J., Sun, Y., Liu, L., Wang, F., Zhao, L., 2011. Comparing Enterovirus 71 with Coxsackievirus A16 by analyzing nucleotide sequences and antigenicity of recombinant proteins of VP1s and VP4s. BMC Microbiol. 11, 246.
Li, J.X., Mao, Q.Y., Liang, Z.L., Ji, H., Zhu, F.C., 2014a. Development of enterovirus 71 vaccines: from the lab bench to Phase III clinical trials. Expert Rev. Vaccines 13 (5), 609–618.
Li, R., Liu, L., Mo, Z., Wang, X., Xia, J., Liang, Z., Zhang, Y., Li, Y., Mao, Q., Wang, J., Jiang, L., Dong, C., Che, Y., Huang, T., Jiang, Z., Xie, Z., Wang, L., Liao, Y., Liang, Y., Nong, Y., Liu, J., Zhao, H., Na, R., Guo, L., Pu, J., Yang, E., Sun, L., Cui, P., Shi, H., Wang, J., Li, Q., 2014b. An inactivated enterovirus 71 vaccine in healthy children. N. Engl. J. Med. 370 (9), 829–837.
Liu, W., Wu, S., Xiong, Y., Li, T., Wen, Z., Yan, M., Qin, K., Liu, Y., Wu, J., 2014. Co-circulation and genomic recombination of coxsackievirus A16 and enterovirus 71 during a large outbreak of hand, foot, and mouth disease in Central China. PLoS One 9 (4), e96051.
Liu, C., Yang, H., Xu, Z., Li, D., Zhou, M., Xiao, K., Shi, Z., Zhu, L., Yang, L., Zhou, R., 2015. microRNA-548 l is involved in the migration and invasion of non-small cell lung cancer by targeting the AKT1 signaling pathway. J. Cancer Res. Clin. Oncol. 141 (3), 431–441.
Louten, J., Beach, M., Palermino, K., Weeks, M., Holenstein, G., 2015. MicroRNAs expressed during viral infection: biomarker potential and therapeutic considerations. Biomark. Insights 10 (Suppl. 4), 25–52.
Mao, Q., Wang, Y., Yao, X., Bian, L., Wu, X., Xu, M., Liang, Z., 2014. Coxsackievirus A16: epidemiology, diagnosis, and vaccine. Human Vaccines Immunother. 10 (2), 360–367.

Mehta, A., Baltimore, D., 2016. MicroRNAs as regulatory elements in immune system logic. Nat. Rev. Immunol. 16 (5), 279–294.
Muehlenbachs, A., Bhatnagar, J., Zaki, S.R., 2015. Tissue tropism, pathology and pathogenesis of enterovirus infection. J. Pathol. 235 (2), 217–228.
O'Connell, R.M., Rao, D.S., Chaudhuri, A.A., Baltimore, D., 2010. Physiological and pathological roles for microRNAs in the immune system. Nat. Rev. Immunol. 10 (2), 111–122.
Piva, R., Spandidos, D.A., Gambari, R., 2013. From microRNA functions to microRNA therapeutics: novel targets and novel drugs in breast cancer research and treatment (Review). Int. J. Oncol. 43 (4), 985–994.
Puenpa, J., Theamboonlers, A., Korkong, S., Linsuwanon, P., Thongmee, C., Chatproedprai, S., Poovorawan, Y., 2011. Molecular characterization and complete genome analysis of human enterovirus 71 and coxsackievirus A16 from children with hand, foot and mouth disease in Thailand during 2008–2011. Arch. Virol 156 (11), 2007–2013.
Schlingmann, B., Molina, S.A., Koval, M., 2015. Claudins: gatekeepers of lung epithelial function. Sem. Cell Dev. Biol. 42, 47–57.
Shan, Y., Zheng, J., Lambrecht, R.W., Bonkovsky, H.L., 2007. Reciprocal effects of micro-RNA-122 on expression of heme oxygenase-1 and hepatitis C virus genes in human hepatocytes. Gastroenterology 133 (4), 1166–1174.
Skalsky, R.L., Cullen, B.R., 2010. Viruses, microRNAs, and host interactions. Annu. Rev. Microbiol. 64, 123–141.
Solomon, T., Lewthwaite, P., Perera, D., Cardosa, M.J., McMinn, P., Ooi, M.H., 2010. Virology, epidemiology, pathogenesis, and control of enterovirus 71. Lancet Infect. Dis. 10 (11), 778–790.
Sonkoly, E., Stahle, M., Pivarcsi, A., 2008. MicroRNAs and immunity: novel players in the regulation of normal immune function and inflammation. Semin. Cancer Biol. 18 (2), 131–140.
Sullivan, C.S., Ganem, D., 2005. MicroRNAs and viral infection. Mol. Cell 20 (1), 3–7.
Tam, A., Wadsworth, S., Dorscheid, D., Man, S.F., Sin, D.D., 2011. The airway epithelium: more than just a structural barrier. Ther. Adv. Respir. Dis. 5 (4), 255–273.
Treiber, T., Treiber, N., Meister, G., 2012. Regulation of microRNA biogenesis and function. Thromb. Haemost. 107 (4), 605–610.
van Zuylen, W.J., Rawlinson, W.D., Ford, C.E., 2016. The Wnt pathway: a key network in cell signalling dysregulated by viruses. Rev. Med. Virol. 26 (5), 340–355.
Wang, C., Guan, S., Chen, X., Liu, B., Liu, F., Han, L., Un Nesa, E., Song, Q., Bao, C., Wang, X., Cheng, Y., 2015. Clinical potential of miR-3651 as a novel prognostic biomarker for esophageal squamous cell cancer. Biochem. Biophys. Res. Commun. 465 (1), 30–34.
Wang, R.Y., Weng, K.F., Huang, Y.C., Chen, C.J., 2016. Elevated expression of circulating miR876-5p is a specific response to severe EV71 infections. Sci. Rep. 6, 24149.
Winter, J., Jung, S., Keller, S., Gregory, R.I., Diederichs, S., 2009. Many roads to maturity: microRNA biogenesis pathways and their regulation. Nat. Cell Biol. 11 (3), 228–234.
Wong, N., Wang, X., 2015. miRDB: an online resource for microRNA target prediction and functional annotations. Nucleic Acids Res. 43 (Database issue), D146–152.
Wu, J., Shen, L., Chen, J., Xu, H., Mao, L., 2015. The role of microRNAs in enteroviral infections. Braz. J. Infect. Dis. 19 (5), 510–516.
Yang, Z., Tien, P., 2014a. [MiR373 and miR542-5p regulate the replication of enterovirus 71 in rhabdomyosarcoma cells]. Sheng wu gong cheng xue bao = Chin. J. Biotechnol. 30 (6), 943–953.
Yang, Z., Tien, P., 2014b. MiR432* regulate the replication of coxsackievirus A16 in rhabdomyosarcoma cells. Wei sheng wu xue bao = Acta Microbiol. Sin. 54 (6), 679–687.
Zhang, C., Chen, F., Han, L., 2015. The cofilin of host cell and infection–a review. Wei sheng wu xue bao = Acta Microbiol. Sin. 55 (12), 1537–1542.
Zhu, Z., Qi, Y., Fan, H., Cui, L., Shi, Z., 2016. Systematic identification and bioinformatic analysis of MicroRNAs in response to infections of coxsackievirus A16 and enterovirus 71. BioMed Res. Int., 4302470.